Competitive Anionic Exchange of Thiolate Ligands onto Aqueous Phosphonate-Capped Quantum Dots

John H. Dunlap, Nuwanthaka P. Jayaweera, Perry J. Pellechia and Andrew B. Greytak*

Department of Chemistry and Biochemistry, University of South Carolina, Columbia, South Carolina 29208.

ABSTRACT: This study examines the relative binding strength of a series of thiolate ligands to the surfaces of zincblende CdSe/ZnS core/shell quantum dots (QDs) passivated by phosphonate ligands under basic conditions in water by means of isothermal titration calorimetry (ITC). A labile hydrophilic intermediate, 2-aminoethylphosphonic acid (AEP), was introduced in place of native hydrophobic carboxylate ligands to produce water-soluble QDs and provide a universal starting point for competitive anionic exchange reactions. We introduce monothiols of different chain lengths, and a dithiol analogue (dihydrolipoic acid), to probe the effects of chain length and denticity on binding strength. Introduction of each of the ligands produces an exothermic response. An increase in chain length among the monothiols led to an increase in the equilibrium exchange constant, $K_{\rm ex}$, indicating longer chain lengths lead to stronger binding. However, the shorter chain mercaptopropionic acid showed greater total exothermicity, which appears to indicate a greater total number of accessible binding sites. Introduction of a dithiol ligand produces a larger $K_{\rm ex}$ than the monodentate thiols, consistent with greater binding strength and stability inferred from previous observations, and ligand density comparable to the shorter-chain mercaptopropionic acid at saturation. This work should aid in the development of stable and versatile water-soluble QD colloids for bioimaging and sensing applications.

INTRODUCTION

Colloidal semiconductor quantum dots (QDs) have emerged as promising fluorescent imaging probes for biological applications due to their enhanced photostability, narrow size-tunable emission spectra, and multifunctional surfaces compared to common organic fluorophores.¹⁻⁵ When a semiconductor QD (such as CdSe, ZnSe, or InP) is overcoated with an inorganic shell (CdS(Se), ZnS(Se), etc.) to produce appropriate core/shell heterostructures, the photoluminescence quantum yield (PLQY) and photostability can be further enhanced due to isolation of potential surface trap states from the excited states centered on the core.6-11 Core/shell structures are widely employed in ODs used for biological applications because they tend to maintain higher PLQYs upon phase transfer into polar/aqueous solvent relative to core-only particles, yet their PLQY typically remains sensitive to surface modification.¹²⁻¹⁵ Achieving appropriate coordination of the inorganic surface of core/shell QDs has been a major focus in developing highly capable QD-based agents for fluorescence microscopy, diagnostics, and sensors in biological applications. Replacing initial coordinating ligands (which are typically hydrophobic) with hydrophilic ones offers a route to aqueous QDs with smaller hydrodynamic size than can be achieved with alternative encapsulation strategies.16-20

Previous studies of ligand exchanges for biological QD applications have typically focused on establishing the feasibility of various strategies for surface coordination,

colloidal stability, linking chemistry, and absence of nonspecific binding. Some strategies include monodentate, polydentate,21 and polymeric ligands22-25 that can coordinate the QD surface while providing anionic, 26 zwitterionic,17,27-29 or steric (e.g. polyethylene glycol, PEG) stabilization.¹⁶ In many cases, thiols are the predominant binder group, chosen for its strong affinity to QD surfaces and relative ease of exchange with native alkylcarboxylate, alkylphosphonate, amine, and phosphine ligands under anhydrous and biphasic conditions. 16,17,26,30,31 To advance the prospects of QDs in aqueous and biological environments, it is necessary to evaluate the complex surface chemistry of ODs under such conditions in an organized, systematic approach that facilitates the creation of more stable, robust, and versatile QD coatings. In particular, there is a growing need to understand the coordination and intermolecular interactions that promote the stabilization of molecular ligands on QD surfaces under these conditions. While thiols can suffer from limitations in terms of fluorescence brightness and stability toward oxidation,12,32,33 they provide a good model for systematic variation of denticity, tail group size, and structure in order to examine their contributions to binding thermodynamics.^{26,34} Additionally, thiols provide access to very small hydrodynamic sizes^{17,35} and are also known as ligands for direct synthesis of QDs in aqueous solvent mixtures.36

Rotello's group found that dithiolate anchors on PEG chains used for steric stabilization lead to greater intracellular stability of CdSe/ZnS vs. monothiolate-capped QDs

of the same size.³⁷ Heyes's group also sought to determine whether mono- or bi-dentate binders were more suitable for biological applications by monitoring binding of thiolated probe molecules (dyes and reduced immunoglobulin G) to CdSe/ZnS QDs capped by monodentate mercaptopropionic acid (MPA) or bidentate, 8-carbon dihydrolipoic acid (DHLA) in neutral aqueous buffer.38 They found an intriguing result: bidentate DHLA was a stronger binder to the OD and better able to resist binding of probes at high probe concentrations, but DHLA suffered from greater probe binding at low probe concentration, an apparent consequence of lower surface coverage by the bidentate ligand that left vacant sites to which probes could easily bind. However, they did not test longer-chain monodentate ligands. Longer alkyl linkers appear to be associated with greater stability of alkanethiolate-coated QDs as recently reported by Heyne et al.34 More sensitive metrics that directly measure ligand association or exchange are necessary to go beyond such rankings and quantify the strength of binding among different binders, but there are relatively few studies that directly study relative binding strengths and quantify ligand exchanges in polar/protic solvents.12,39,40

In this study, the ligands 3-mercaptopropionic acid (MPA), 11-mercaptoundecanoic acid (MUA), and dihydrolipoic acid (DHLA) were introduced as thiolates to the QDs coordinated by 2-aminoethylphosphonate (AEP) in aqueous mildly basic aqueous buffer (**Scheme 1**). We monitored this competitive exchange by NMR and isothermal titration calorimetry (ITC) to examine how increases in alkyl chain length and/or substitution of a bidentate anchor group influence the association constants for thiolate ligands to QDs under aqueous conditions.

Scheme 1. Phosphonate to thiolate ligand exchange reactions

Isothermal titration calorimetry (ITC) is a well-known biochemical technique used to characterize the thermodynamics of binding interactions to proteins and other biological substrates.⁴¹⁻⁴⁴ Recently, ITC has been applied to coordination of nanocrystal surfaces such as Au nanoparticles and CsPbBr₃, InP, and CdSe, and CdSe/CdZnS QDs.⁴⁵⁻⁵⁵ ITC offers some advantages over common spectroscopic metrics and is not limited to deuterated solvents, spectroscopic handles, or high sample concentrations. Through a single and direct measurement, the enthalpy change, equivalency, and binding constant may be obtained.⁵⁶ However, the signal measured is sensitive to contributions from all processes or reactions taking place during the titration, thus complementary techniques

(such as NMR) are often required to characterize the reactants and final products.

Ligands for aqueous QDs generally consist of a binding headgroup, a hydrophilic tail group, and a spacer (such as an alkyl chain) between the two, 16 all of which may have some contributions to the enthalpy and entropy of binding through coordination, interligand, and ligand-solvent interactions. Such interactions may vary with QD composition, crystal structure, size, or shape. Therefore, systematic studies on the independent influence of each moiety are necessary to establish how ligands bind and what leads to stronger binding. Rioux's group investigated the effect of chain length on the adsorption of alkane thiols with carboxylic acid binders (including MPA) to Au nanoparticles (NPs) in water.46 The binding appeared to be enthalpically-driven, and increasingly exothermic with increasing chain length (C2-C6) regardless of Au NP diameter (5-20 nm). The effect of alkyl chain length for monothiols has also been described by Elimelech et al. on oleate-capped CdSe QDs in trichloroethylene.53 There, increases in chain length also contributed to greater exothermicity, with compensation by greater entropic loss observed at longer chain lengths where ligands passivate the QD less efficiently due to steric effects. Recently, this work has been extended to comparison of branched and linear thiols, in which branched alkylthiols were found to suffer a smaller entropic penalty on exchange onto the surface.57 Most ITC studies with QDs have been limited to nonpolar or weakly polar solvents, where it is known that thiolates bind strongly to surface atoms and displace carboxylates in approximately 1:1 stoichiometries (an example of X-type ligand exchange⁵⁸). This may not be the case in aqueous solution where water can solvate charges and the pH can strongly influence the protonation states and binding of ligands. 12,39.59 There is a need to extend our understanding of ligand binding to this regime relevant to bioimaging. Here, we quantify the relative binding strengths of thiolate ligands with different alkyl chain lengths and denticity to CdSe/ZnS core/shell ODs in aqueous buffer.

To effectively describe the relative binding of thiolates by ITC, a homogeneous solvent is required. However, direct replacement of native ligands such as oleate with thiols is often conducted via biphasic reactions or in organic solvents and while effective, it would be advantageous to describe such exchanges in aqueous solvents. Recently, the Weiss group reported the formation of water-soluble CdSe and CdS QDs through X-type oleate to phosphonate exchange, with a view toward photocatalytic applications.^{39,40,59,60} 2-aminoethylphosphonic acid (AEP) was shown to be a labile ligand that provided several days of colloidal stability under basic conditions via electrostatic stabilization.40 We reasoned that AEP-capped core/shell ODs could serve as a starting point for investigating ligand exchanges in water, with AEP effectively serving as a leaving group. As a strategy for investigating the relative binding strength of thiolates, this approach has several advantages compared to investigating exchanges from one thiol to another. Firstly, as seen below, AEP to thiolate exchange is strongly exothermic, producing a signal that is easily distinguished from heats of dilution and probes the difference in enthalpy for phosphonate vs. thiolate coordination in aqueous buffer. Secondly, examining a reaction with a larger value of the exchange equilibrium constant $K_{\rm ex}$ facilitates finding unique solutions for $K_{\rm ex}$, the number of sites N, and the average enthalpy change ΔH . 61

Thiols possess lone pairs in addition to a moderately acidic proton, and as such can in principle function as neutral nucleophilic (L-type) ligands in their protonated form, or as X-type thiolates. 12,58,62 The latter case appears to predominate in several examples of thiol ligand coordination in polar and non-polar solvents. 12,53,63 To simplify the analysis in the present case, reactions were conducted in moderately basic borate buffer (pH ~9.2), which is above the typical pKa for thiols and carboxylates in water, and is also a regime in which the AEP-QDs are relatively stable. The zincblende crystal structure was selected due to greater symmetry versus wurtzite QDs, which could simplify interpretation of surface sites⁶⁴ and could be achieved with pure carboxylate (oleate) native ligands. Overcoating of a ZnS shell onto zincblende CdSe was achieved by a successive ionic layer adsorption and reaction (SILAR) process. 65,66 We prepared AEP-QDs through a biphasic exchange of native oleate ligands with 2aminoethylphosphonic acid (AEP) under basic conditions, and ITC titrations were conducted in the presence of an excess of AEP to maintain colloidal stability of the AEP-QD intermediate.

As described below, in each case, an exothermic signal corresponding to quantitative ligand exchange was observed. In the case of the monothiolates, we observe a smaller total exothermic response per OD for MUA versus MPA. In contrast, exchanging the AEP with DHLA led to a more negative total heat than either of the monothiolates. Each titration was analyzed in terms of an empirical thermodynamic model of identical, independent sites (effective Langmuir isotherm) with the number of sites, enthalpy, and effective association constant as model parameters. Exchanges were conducted in the presence of a known concentration of excess AEP, enabling recovery of the exchange equilibrium constant, K_{ex} . We found that K_{ex} increases with increasing chain length, and is also significantly larger in the case of the bidentate DHLA. Despite this, the total enthalpy change for saturation of the QDs with MUA is less negative than that of MPA, suggesting that the larger K_{ex} for the longer chain ligand is accompanied by a smaller number of accessible sites and/or less negative entropy change when it replaces AEP on the QD surface.

METHODS

Optical Spectroscopy. Absorption spectra were recorded with a Thermo Scientific Evolution Array UV-Visible spectrophotometer in a quartz cuvette with a path length of 1-cm. Emission spectra were recorded with an Ocean Optics USB 4000 spectrometer equipped with a

365 nm fiber-coupled light emitting diode excitation source.

NMR Characterization of Ligands and QDs. 1H and ³¹P NMR measurements were conducted on a Bruker AVANCE III-HD 500 MHz spectrometer. The measurements for the free AEP ligand at different pH values was measured on a Bruker AVANCE III-HD 400 MHz spectrometer. The 1x PR QDs and hexane washes from ligand exchanges were prepared by drying the samples and dispersing in toluene- d_8 with a hexamethylcyclotrisiloxane (HMCTS) internal standard. Thiolate- and phosphonatecapped QDs were prepared for NMR by centrifugal dialysis and dilution with D2O. 1,4-dioxane was used as an internal standard for all QD measurements in D2O. Reference measurements of oleic acid and free ligands in D2O were basified to pH ~ 9.3 with potassium carbonate (0.2 M K₂CO₃ in D₂O). ¹H NMR measurements in toluene-d₈ and D₂O were conducted with a 11 s and 30 s delay, respectively (at least 5 x T₁). ¹H NMR in D₂O used a presaturation solvent suppression pulse sequence due to the significant presence of water in the samples. 31P measurements were proton decoupled with 256 scans and a 1s delay time.

Powder X-ray Diffraction Measurements. Diffraction experiments were performed using a Bruker D8 Ouest single crystal X-ray diffractometer equipped with a microfocus Mo K α X-ray source (λ = 0.71073 Å) and a Photon II detector. Approximately 7-10 mg of CdSe cores and CdSe/ZnS QDs were purified by 1x PR into hexanes and dried under vacuum for 1 hour to obtain a viscous oil. The concentrated QD solution was loaded into a 0.81 mm ID polyimide tube and mounted in the diffractometer. A series of five phi scans (image width = 360°) were then collected with different detector orientations covering a 2θ range of 0-40° at a detector distance of 100 mm. These images were merged and integrated into a 2D powder diffraction pattern using the Bruker APEX3 software. QD powder patterns were compared to zincblende CdSe (ICSD #41528) obtained from the Inorganic Crystal Structure Database (ICSD).

Scanning Transmission Electron Microscopy (STEM). CdSe/ZnS QDs were purified by 1x precipitation and redissolution (PR) into hexanes and drop cast onto a TEM grid (Ted Pella Inc., Type A, 400 Mesh Cu grid with Formvar and ultrathin carbon support film) and dried under vacuum for 1 hour. The samples were imaged on a JEOL 2100F 200 kV FEG-STEM/TEM. Samples were preirradiated by an electron beam shower for 15 minutes prior to imaging to polymerize hydrocarbons on the film and improve sample quality at high magnification. High angle annular dark field (HAADF) images were obtained via a Fischione model 3000 HAADF detector between 75-300 mrad. The convergence semi-angle of the probe was 17.5 mrad. Images were acquired synchronously with a 60 Hz AC electrical line frequency to minimize 60 Hz noise in the images.

Synthesis of Zincblende CdSe QD Cores. Oleate-capped CdSe cores were synthesized following a previous-

ly published procedure.52 In brief, 120 mg CdO was dissolved in 660 mg oleic acid (99%) and 12 mL ODE in a three-neck round bottom flask. The mixture was degassed at 100 °C under vacuum to remove water and oxygen, then heated under N2 to 270 °C to form cadmium oleate (Cd(OA)₂) as a clear and colorless solution. The reaction mixture was cooled to ~130 °C and evacuated to remove adventitious water, then heated to 270 °C under N2. At 270 °C, 1.28 mL of a 2.2 M TOPSe precursor was rapidly injected, and the reaction mixture immediately quenched with a cool air gun. QDs were isolated from the flask with a minimal hexane rinse and stored in the dark under air. The radius of the CdSe core (1.91 nm) was determined based on an established size calibration curve by Kuno using the 1st excitonic peak position and quantity of the CdSe cores (546 nm).67

Synthesis of Zincblende CdSe/ZnS Core/Shell QDs. Zincblende, oleate-capped CdSe/ZnS QDs were prepared by a modification to previously reported SILAR method.⁶⁸ Our modifications were the use of zincblende, oleatecapped CdSe cores and lower sub-monolayer equivalencies (0.533 ML/cycle). The CdSe cores were purified by 1x PR with Acetone/MeOH into a known volume hexanes and the amount and size of the cores quantified by absorption spectroscopy and established sizing curves. The cores were diluted into a 2:1 v/v mixture of ODE/THA and degassed at 80 °C for 2 hours to remove hexanes and air. The reaction mixture was heated under N2 to 200 °C (growth temperature). The Zn metal precursor was prepared by diluting 2.2 M Zn(OA)₂ in TOP with THA to a total Zn concentration of o.1 M. The sulfur precursor was prepared by diluting (TMS)₂S in TOP to a total S concentration of o.1M. Precursors were introduced by alternating injections of the metal and chalcogenide reagents at 0.533 monolayer equivalents per cycle via a syringe pump (J-KEM Scientific Dual Syringe Pump, model 2250). Injections were performed over 3 minutes, followed by 12 minutes of equilibration time. Core/shell samples were stored at room temperature under air in the dark.

Direct Carboxylate to Thiolate Exchange. Direct exchange of carboxylates for thiolate ligands on core/shell QDs were performed via biphasic exchange. The amount/equivalents of thiolate ligand used was determined by the mole ratio of total thiolate ligand present in the active cell volume at the end of the ITC titrations to the moles QDs in the titrations. Methanolic solutions of MPA, MUA, and DHLA were prepared and basified with KOH (2:1 KOH/Thiol mole ratio). The QDs were purified by 1x PR into hexanes and the amount of QDs quantified by absorption spectroscopy. The ligand exchange was performed by adding the QD solution in hexanes to the ligand solutions in MeOH and stirring at room temperature for 3 hours in the dark. Following the exchange, the thiolate-capped ODs were centrifuged to remove poorly dispersed particles and washed with 3x 4 mL hexanes to remove displaced oleate/potassium oleate. MeOH/hexane layers were allowed to separate before pipetting away the top hexane layer and proceeding to the next wash, and all washes combined and saved for further

analysis. After the washes, the QDs were centrifuged once more, the supernatant decanted to waste, then dried under vacuum on a Schlenk line. The dried QDs were finally dispersed in borate buffer (pH 9.18) and stored under air in a dark refrigerator.

To prepare the thiolate-capped QDs for NMR and optical analysis by removing weakly-bound or excess ligands, we performed centrifugal dialysis using Vivapsin Turbo 4 spin concentrators with a polyethersulfone membrane (50 kDa MWCO). The filters were preconditioned with DI water and borate buffer to wash the membranes prior to use with the QDs. Thiolate-capped QD samples were concentrated by 1x centrifugal filtration (5000 rpm/5 min), then diluted with borate buffer and dialyzed once. The retained QDs were diluted with borate buffer for optical measurements. For NMR, samples were further diluted with D2O. 1,4-dioxane was used as an internal standard for aqueous NMR measurements.

Carboxylate to Phosphonate Ligand Exchange. AEP-capped QDs were prepared by biphasic ligand exchange following a modified procedure by Arcudi et al.40 An AEP stock solution was prepared by dissolving the AEP and KOH (at a 3:1 KOH:AEP mole ratio) in MeOH to form a 0.04 M AEP solution. The QDs were purified by 1x PR into a known volume of hexanes and quantified by absorption measurements. 1100 equivalents of AEP per mole QD was injected into the QD solution, inducing flocculation and phase transfer of the QDs from hexane to methanol upon ligand exchange. The biphasic mixture was centrifuged at 9500 rpm/5 min to ensure complete separation of the hexanes and MeOH. The hexane supernatant containing impurities and excess native ligand was removed by glass pipette, then the AEP-QDs were washed three times with hexane. Each wash was performed by adding 2 mL hexane to the QDs, mixing, and centrifuging at 9500 rpm/ 5 min to achieve phase separation before subsequent removal of the supernatant. All hexane washes were combined and saved for further analysis. After the final wash, the QDs were dried under vacuum on a Schlenk line to remove MeOH and redispersed in borate buffer.

For a parallel NMR experiment, the AEP exchange was accomplished as described above. The QDs in borate buffer were further diluted with D₂O and 1,4-dioxane (internal standard) to form an 80:20 v/v buffer/D₂O mixture.

For the ITC experiments, the QDs were further diluted with a 6.73 mM AEP/borate buffer solution (pH 9.17) such that the nominal concentration of AEP in the QD sample was between 12-13.14 mM. The neat AEP-QDs in AEP buffer were used in the ITC titrations without further purification.

Phosphonate to Thiolate Exchange for NMR. AEP-QDs were prepared as described above. Thiolate ligand stock solutions were prepared by diluting the thiol ligand in borate buffer and adjusting basifying with KOH to pH 9.15-9.18 and a nominal concentration of 5 mM. For a given exchange, the amount of thiolate ligand to introduce to the AEP-QDs was determined by the mole ratio of total

thiolate ligand present in the active cell volume at the end of the ITC titrations to the moles QDs in the titrations. The thiolate ligand in borate buffer was introduced to the AEP-QDs and stirred at room temperature in the dark for 3 hours. Samples were purified by dialysis using centrifugal spin concentrators as in the direct thiolate exchanges described above. The retained thiolate-QDs were isolated and diluted with D_2O and 1,4-dioxane was included as an internal standard to form an 80:20 v/v buffer/ D_2O mixture.

Photoluminescence Quantum Yield (PLQY). The PLQY of the QD samples was measured relative to a rhodamine 640 perchlorate standard (R640, PLQY reported as 100% in ethanol). Fluorescence spectra were measured using a Horiba Scientific FluoroMax Plus spectrofluorometer. The PLQYs for the QDs before and after ligand exchange are listed in **Table S1** in the Supporting Information.

Isothermal Titration Calorimetry. ITC titrations were performed in a TA Instruments Affinity-ITC Low-Volume (LV) calorimeter under air at 25°C. The thiolate ligand solutions (ligand in neat borate buffer at pH 9.15-9.18) were titrated from a 250 µL syringe into a gold sample cell containing 350 µL of QDs in AEP buffer. The active cell volume of the cell was 185 µL. The power compensation required to maintain the sample cell at 25 °C (relative to a reference cell filled with an equal volume of pure DI water) was monitored over time with each injection. All experiments allowed for a midrange power variation. Each injection was followed by a 300 s interval to allow proper equilibration between ligand injections, with a total of 30 injections of 5 µL each. The cell contents were stirred continuously at 150 rpm over the course of the titration. The ligand solutions were sparged with N₂ and stored under N₂ atmosphere in the dark prior to each experiment to limit thiol oxidation. Reference titrations of neat buffer-to-buffer and thiolate ligand-to-AEP buffer were conducted under identical parameters as the ligandto-QD titrations. The sample cell was thoroughly cleaned with buffer or AEP buffer before each titration. Ligand-to-AEP buffer reference experiments were conducted before the ligand-to-QD runs to account for potential thiol association to the cell by saturating any possible gold sites.

RESULTS AND DISCUSSION

Preparation of AEP-Capped Core/Shell QDs. Many previous investigations of ligand exchange on CdSe-based core/shell QDs employed wurtzite structures. We thought it would be beneficial to investigate ligand exchanges on QDs with higher symmetry to facilitate interpretation of surface sites and as a model system for other zincblende nanocrystals including those based on III-V core compounds. The influence of ligands used in synthesis on the crystal structure of CdSe QDs has been noted in previous reports: alkylcarboxylate ligands tend to produce zincblende QDs, while alkylphosphonates tend to enforce wurtzite QD formation.⁷⁰ Wurtzite core/shell QD preparations have the potential for phosphonic acid anhydride ligands (such as tetradecyl phosphonic acid anhydride) to

persist after shell growth. In contrast, zincblende syntheses result in QD cores capped purely with carboxylate ligands, as well as cubic symmetry, which is advantageous for investigating ligand exchange chemistries. We chose SILAR as the synthetic method due to its ability to produce QDs with quasi-spherical morphologies and high PLQYs. The oleate-capped CdSe/ZnS core/shell QDs (OA-QDs) were prepared similarly to our previous reports,⁶⁸ with minor modifications: (1) the use of zincblende CdSe cores to promote epitaxial growth of a zincblende ZnS shell, in contrast to most previous colloidal SILAR studies which have employed wurtzite, and (2) using lower submonolayer equivalencies per cycle (~0.533 ML equivalents/cycle) to achieve a narrow size distribution by suppressing homogeneous nucleation of the shell material as ZnS particles. The PLQY of the OA-QDs in hexanes was measured to be 96.6 %. The oleate-capped core/shell QDs were purified by flocculation with acetone and methanol followed by redispersion in hexanes prior to ligand exchange or further analysis. Figure 1 shows the initial characterizations of the OA-QDs. The crystal structures of the core and core/shell samples were confirmed to be zincblende by powder X-ray diffraction (PXRD). Upon overcoating of the ZnS shell, we observe a shift in lattice parameter due to compression of the CdSe core, indicated by a slight shift in peak position, confirming that shell growth proceeded epitaxially. We further characterized the QDs by scanning transmission electron microscopy (STEM) to determine the average radius of the core/shell particles (2.21 nm). The radius of the CdSe core (1.91 nm) was determined based on an established size calibration curve by Kuno using the 1st excitonic peak position (546 nm) and quantity of the CdSe cores.⁶⁷

Scheme 2. Oleate to Phosphonate Ligand Exchange Procedure.

Aqueous AEP-QD dispersions were achieved through successful ligand exchange of the native hydrophobic carboxylate ligands as described in **Scheme 2.** Our procedure follows that of Weiss and coworkers, however at a higher equivalency (1100 equivalents of AEP per mole QD) to help drive displacement of the native oleate ligands. Introduction of a methanolic solution of AEP and KOH induced flocculation of the OA-QDs from hexanes, followed by phase transfer into methanol with ligand exchange. The AEP-QDs were then washed several times

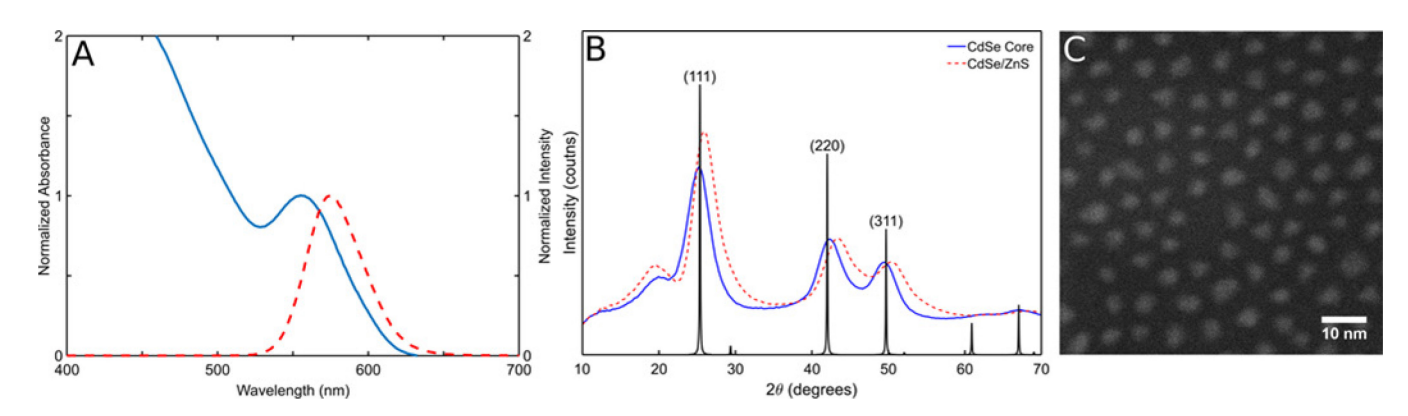


Figure 1. Characterization of oleate-capped CdSe/ZnS QDs. (A) Absorption (blue, solid) and emission (red, dashed) spectra of QDs in hexanes normalized to the peak maxima. (B) Powder X-ray diffraction patterns of the zincblende CdSe core (blue, solid) and CdSe/ZnS core/shell QD (red, dashed), and a reference pattern for bulk zincblende CdSe (black, ICSD #41528). (C) HAADF-STEM image of the CdSe/ZnS QDs.

with hexanes to remove displaced oleate and dried under vacuum to evaporate the methanol. The final AEP-QDs could be dispersed in borate buffer (pH ~9.2) and remained stable under air for several days.

While the phase transfer from nonpolar to polar solvent with introduction of AEP indicated a change in the QD capping layer, we monitored the phosphonate exchange by ¹H and ³P NMR to determine whether the AEP effectively displaced the native oleate ligands.

Figure 2 shows the initially purified QD sample (blue trace), containing both a broad and slightly sharper resonance at ~ 5.6 ppm indicative of bound and free populations of oleate ligands on and off the QD surface.71 The oleate ligand population was determined to be 242 ligands per QD (Table S2), with a density of 3.9 oleates per nm² in the initial OA-QD sample. Octadecene (ODE) from synthesis was also present that persisted through initial purification. The NMR spectrum of AEP-exchanged QDs (purple trace) in aqueous buffer after several hexane washes is also provided in Figure 2, and the appearance of AEP peaks was noted at 1.6 and 2.9 ppm, along with significant reduction of the olefin species. The hexane washes after AEP exchange were sufficient to remove the native carboxylate ligands displaced by AEP, as well as ODE, yielding AEP-QDs suitable for aqueous ligand exchange experiments (as observed in Figure So). We note that the AEP-QDs retain a broad peak at 5.3 ppm, near the olefin resonances found in the OA-QD samples. This peak, along with a very broad signal at 1.25 ppm, is attributed to the presence of oleate micelles in the AEP-QD sample that are not bound to the QD, as these are also seen in oleic acid samples brought to basic pH in D2O (**Figure S8**). Evaluation of the ³¹P NMR spectra of the OA-QDs in Figure 2 to the AEP-QDs, demonstrates complete removal of tri-n-octylphosphine (TOP), a nucleophilic coordinating solvent employed in shell growth, by the washing step (Figure S10) and the presence of AEP. It should be noted that strongly bound ligands on nanocrystal surfaces tend to have broadened resonances due to slower rotational diffusion relative to freely diffusing ligands in solution.72 In the case of AEP, we observe some broadening, however to a lesser extent than seen in other QD systems, and indeed for AEP-QDs prepared by Weiss and co-workers.⁴⁰ This is due to the large excess of AEP used to accomplish the ligand exchange, as well as the minimal purification conducted on the samples, leading to a large fraction of free AEP in solution that exchanges rapidly with the surface-bound population. We found that a similar synthetic approach could also be used to directly install each of the thiolate ligands investigated here, starting from OA-QD, as described in supporting information (**Figure S21-S23**). This supports our interpretation of thiolates binding as X-type (anionic) ligands under basic conditions, consistent with previous studies emphasizing the success of thiolate exchange under basic conditions and/or when introduced as a zinc salt.⁶³

Phosphonate to Thiolate Exchange. Prior to conducting thermodynamic measurements by ITC, we evaluated AEP to thiolate exchange on the benchtop to confirm that it occurs rapidly under basic conditions in buffer. Solutions of MPA, MUA, and DHLA were prepared by dissolving the free ligand into borate buffer at pH 9.15-9.18. To set up the reaction as a competitive exchange from an AEP-saturated initial state, the AEP-QDs were diluted with a 6.73 mM AEP solution in borate buffer to achieve a total AEP concentration of nominally 13 mM. The thiolate ligand stock solutions were introduced to the AEP-QDs and stirred for 3 hours at room temperature in the dark. Conducting the exchange under basic conditions should favor deprotonated thiolates binding as Xtype ligands to the OD surface. Following ligand exchange, the thiolate-QDs were purified by one cycle of dialysis in centrifugal spin concentrators to remove free thiolates and displaced AEP from the solution. The minimal dialysis purification was successful for the MUA- and DHLA-QDs, however in the case of MPA-QDs, their poor dispersibility resulted in significant sample loss and they were not robust towards purification after thiolate exchange. We initially characterized the product of the ligand exchanges using absorption and PL spectroscopy, shown in Figure 3 for the representative case of DHLA exchange. Displacement of oleate to prepare AEP-QDs resulted in a high-scattering product and a red shift in the absorption and emission, indicative of some degree of aggregation among QD-AEP in aqueous buffer. Both of these changes are reduced significantly after exchange with DHLA and purification. The reduction in scattering upon introduction of the thiolate indicates better colloidal dispersion consistent with ligand exchange.

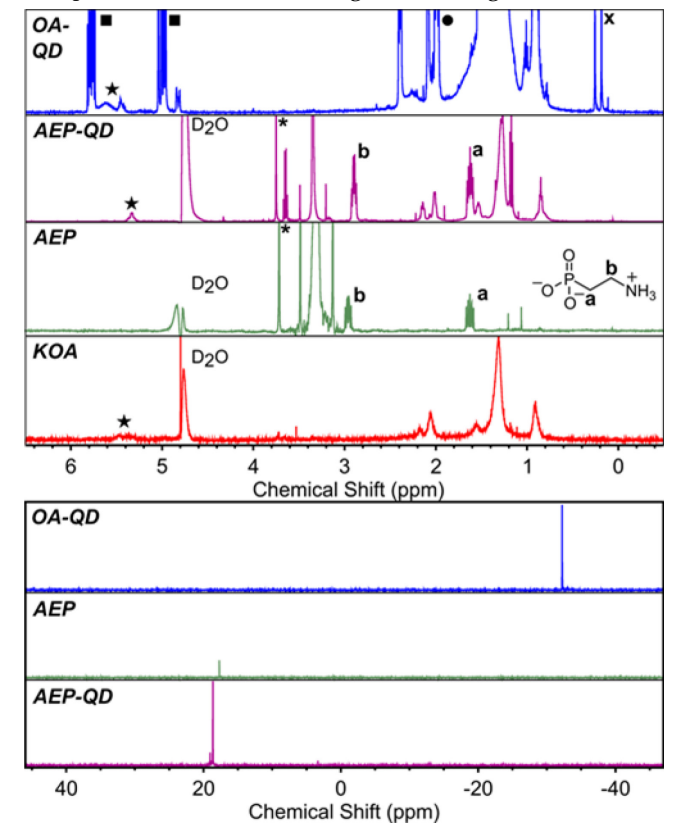


Figure 2. 1 H (top) and 3 P (bottom) NMR spectra of QDs and ligands showing displacement of oleate by AEP. 1 H NMR measurements of aqueous samples were conducted with presaturation solvent suppression to minimize the intensity of the water ($D_{2}O/HOD$) peak at 4.9 ppm. Features at 3.3 ppm in AEP-QD and AEP ligand spectra are associated with methanol from the AEP stock solution used in ligand exchange. The peaks for the internal standard 1,4-dioxane (*) or hexamethylcyclotrisiloxane (X), toluene (\bullet), ODE (\blacksquare), and OA (\bigstar) are indicated. 1 H NMR in $D_{2}O$ used a presaturation solvent suppression pulse sequence due to the significant presence of water in the samples. Full NMR spectra are provided in the Supporting Information.

NMR spectra for the case of AEP to DHLA exchange are presented in **Figure 4**. Treatment with DHLA resulted in a significant reduction of the AEP resonances, indicating successful displacement. Observation of the ³¹P NMR shows the presence of some residual AEP in the DHLA-QD sample, though the peak intensity is greatly diminished with respect to the AEP-QDs. We attribute this reduction to displacement by DHLA, which would result in a decrease in the bound population of AEP. The presence of AEP here is most likely due to the minimal purification used to prepare the DHLA-QDs for analysis, and further purification should effectively remove all free AEP in solution that was retained. We chose to use a minimal purification by centrifugal dialysis here to limit sample loss due

to QD aggregates, because while the scattering for DHLA was quite low, the monothiol-capped QDs were not as well dispersed and prone to sticking on the centrifugal dialysis filter membrane.

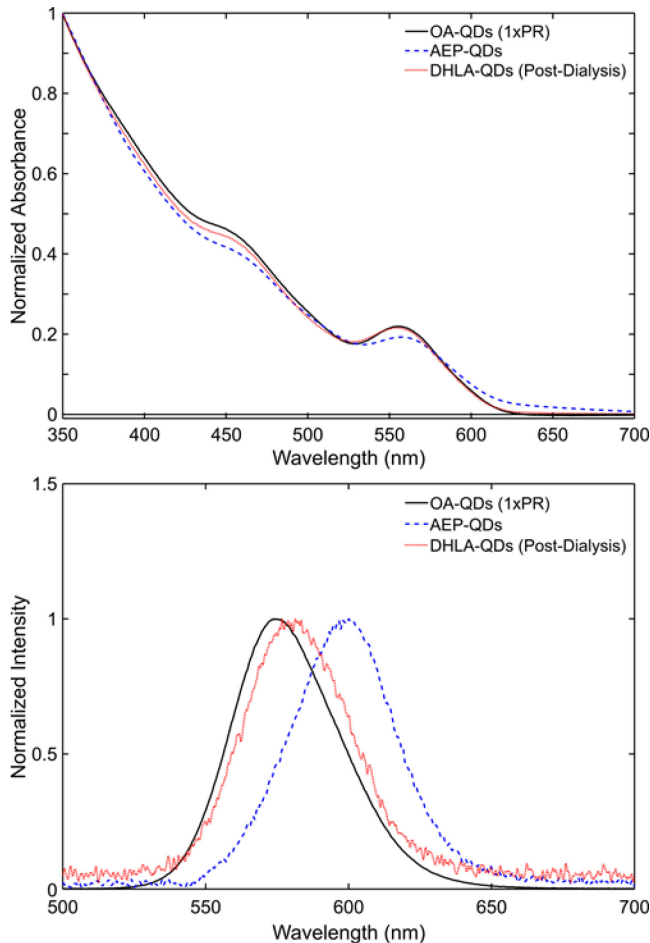


Figure 3. Absorption (top) and emission (bottom) of ligand-exchanged QDs. The absorption spectra are normalized to the absorbance at 350 nm, and emission spectra are normalized to the emission maximum.

Isothermal Titration Calorimetry. Once we had confirmed that the thiolate exchanges occurred, we designed a competitive exchange titration experiment to probe the thermodynamics of the thiolate exchanges to AEP-QDs to determine their relative binding strengths. For each titration, solutions of the thiolates (each prepared at ~12-13 mM in borate buffer) were sparged with N₂ prior to loading into a titrant syringe under air. The sample cell was filled with 350 μL of AEP-QDs (5.2 - 7.5 μM), in buffer containing ~ 13 mM AEP. After equilibration, the titrations were conducted with a series of 30 injections of 5 µL each. Analysis was performed on triplicate runs for each reaction. Background runs from titration of the corresponding thiolate into QD-free AEP buffer solution, recorded under identical conditions, showed smaller exothermic signals attributed to heat of dilutions and slow oxidation of the thiolate ligand; these were subtracted from the QD-ligand signals in each case to isolate the ligand exchange contribution.

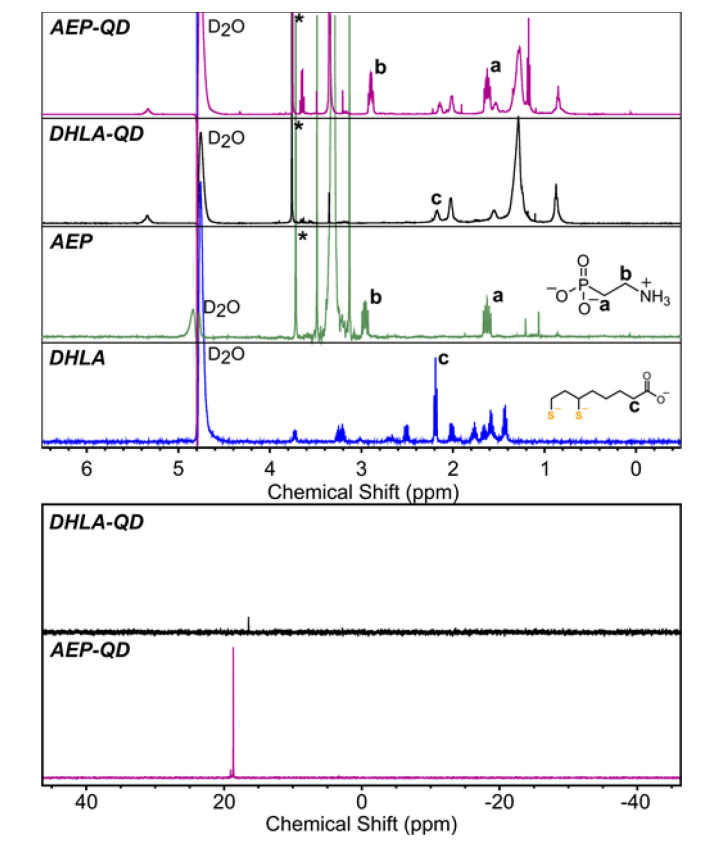


Figure 4. 1 H (top) and 3 P (bottom) NMR of AEP-QDs before and after exchange with DHLA in $D_{2}O$. Peaks for the internal standard are indicated by (*). Full NMR spectra are provided in the Supporting Information.

Figure 5 shows the background-subtracted thermograms and the integrated isotherms for each set of ligand titrations. The isotherms indicate the enthalpy change (Δ*H*, plotted as kJ per mole of ligand added) for each step, and are plotted versus the mole ratio of thiolate/QD. Near the start of each titration, each thiolate injection generates a sharp exotherm that quickly relaxes to equilibrium. Past a mole ratio of a few hundred ligands/QD, these signals subside, indicating the ligand exchange reaction has been saturated. In each case, the ligand-to-QD signals greatly exceed the background at the start of the titration (raw thermograms and background are shown in Supporting Information, **Figure S4**). Below, we analyze the isotherms in terms of an independent-site model, with effective parameters summarized in **Table 1**.

In the simple case of association of a ligand (L) to vacant sites (S), the binding equilibrium may be interpreted as follows, with the effective equilibrium association constant, K_a , determined by the fractional occupation θ of sites by ligand, and ligand concentration [L]:

$$S + L = SL \tag{1}$$

$$K_{\rm a} = \frac{\theta}{(1-\theta)[L]} \tag{2}$$

This analysis can be extended to the case of binding to nanoparticles that each have some number of identical and independent sites (Langmuir model), and within this model, the number of sites (N), enthalpy change (ΔH),

and association equilibrium constant (K_a) can be obtained from least squares fitting of an experimental ITC isotherm. Our case differs in that we are conducting a ligand exchange in which we presume AEP is being displaced. If we assume a negligible fraction of vacant sites, the progress of the reaction can still simply be described by the fractional occupation θ of sites by the new ligand L, but the fractional occupation depends on both the concentration of new ligand [L] and the concentration of the initial ligand [L₁]. For a 1:1 exchange, we define the exchange equilibrium constant $K_{\rm ex}$:

$$K_{\rm ex} = \frac{\theta}{1-\theta} \times \frac{[L_1]}{[L]} = \frac{K_{\rm a,L}}{K_{\rm a,L_1}} \tag{3}$$

In our experiment, we employ a high concentration of the AEP (L_1) to help ensure this limit of saturation (where the fractional occupation of unsaturated sites is negligible), so that we only detect exchange of AEP by the thiolate. We note that in the case where the concentration of free L_1 is much greater than the total concentration of binding sites ($[L_1] \gg N[M]_t$), the fractional change in $[L_1]$ over the course of the exchange reaction is small and $K_{\rm ex}/[L_1]$ has an approximately constant value, which enables us to define an effective association constant $K_{\rm a,eff}$ for the new ligand L in the presence of this concentration of L_1 :

$$K_{\text{ex}}/[L_1] = \frac{\theta}{1-\theta} \times \frac{1}{[L]} = K_{\text{a,eff}}(4)$$

Conveniently, the effective association constant, $K_{a,eff}$, may be determined from analysis of the experimental isotherm according to the Langmuir model, along with N and ΔH. With knowledge of [L₁], the exchange equilibrium constant $K_{\rm ex}$ may then be obtained and used to compare the binding strength of each thiolate compared to AEP. The ratios of K_{ex} for the different thiolates can be used to compare their relative binding strength. As seen in Figure 5, the experimental isotherms can be well described by fits of the Langmuir model, particularly in the case of the MUA and DHLA titrations. The curvature of the MPA isotherm is quite shallow relative to MUA and DHLA, indicating that MPA has a lower affinity to the QD surface. We note that isotherm curve shapes within in the Langmuir model are parameterized by a single value, the Brandt's *c*-parameter, but for values of c < 1 it becomes challenging to obtain unique fits for N and ΔH in the presence of noise.56

$$c = K_{\text{a.eff}} \times N \times [M]_{\text{t}} \tag{5}$$

In the case of MPA, the c parameter for optimized fits is quite low ($c\approx1$) in comparison to that of MUA ($c\approx7$) and DHLA ($c\approx18$). In the limit of low c, fit values for N and ΔH are correlated but their product $N\Delta H$, which describes the total enthalpy change per QD, and $K_{a,eff}$ may still be resolved from the data.

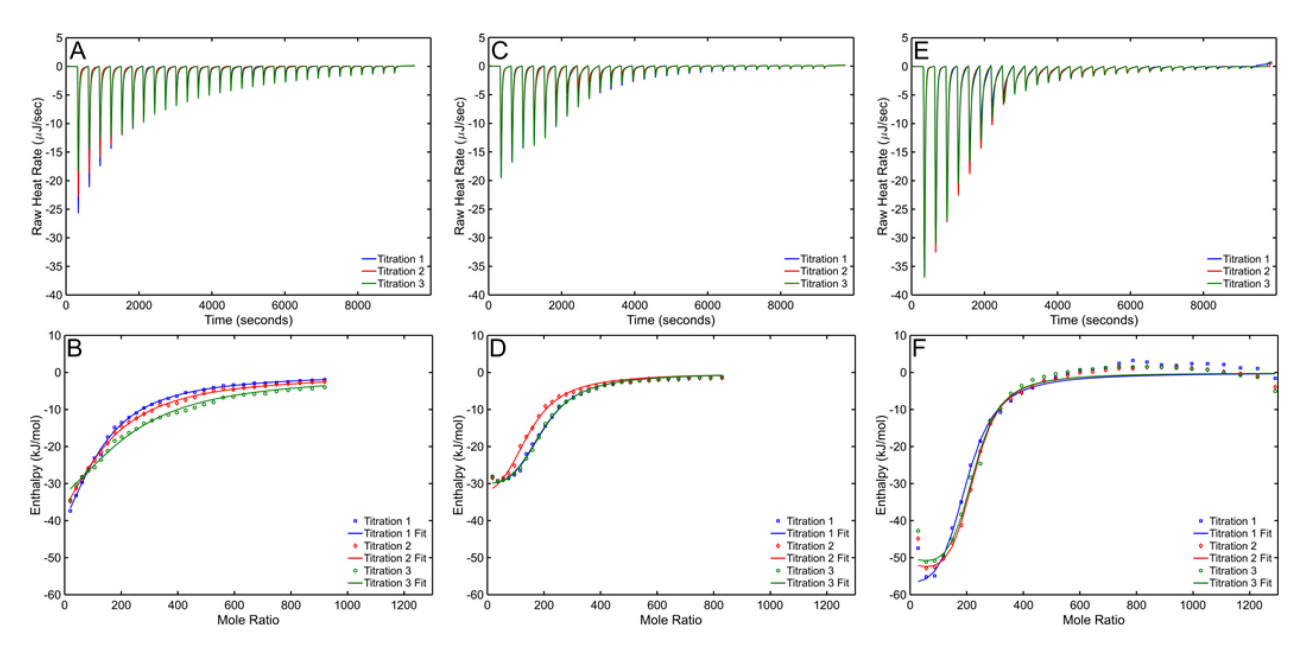


Figure 5. Corrected heat response thermograms (top) and integrated heat isotherms (bottom) of three replicate thiolate titrations. The corrected thermograms were background subtracted and baseline corrected. (A, B) MPA titrations. (C, D) MUA titrations. (E, F) DHLA titrations.

One can also express the relative binding strength of the thiolates by comparing the effective dissociation constant, $K_{d,eff}$, which is calculated by the inverse of $K_{a,eff}$ and represents the free thiolate concentration at which half the sites are occupied by the thiolate:

$$K_{\rm d,eff} = \frac{1}{K_{\rm a,eff}}$$
 (6)

We obtained $K_{\text{d.eff}}$ values of 2, 0.2, and 0.06 mM for MPA, MUA, and DHLA, respectively. This suggested that monothiolates were indeed weaker binders than the bidentate ligand, and that increased chain length improves strength of binding. We note that phosphonopropionic acid (PPA), a weaker-binding analogue of AEP, was estimated to have dissociations constants $K_d \sim 14-2500 \mu M$ in aqueous solution,³⁹ which would place the dissociation constants for the thiolates studied here in the low micromolar range in borate buffer alone. The values for the total enthalpy change per QD, and for $K_{\rm ex}$, are summarized in **Figure 6**.

Comparing the monothiolate ligands, a significantly larger $K_{a,eff}$ and K_{ex} are observed for 11-carbon MUA than for 3-carbon MPA, indicating that MUA is the stronger binder: this is easily seen from the isotherms as the MUA titration saturates more rapidly. The ligand equivalency for MUA, *N*≈166/OD, is larger than that observed in NMR following separation of unbound MUA, but lower than that for the native oleate coating. Comparison of ΔH between the two cases is complicated by the low c parameter in the case of MPA, with wide distributions of optimized values among replicates and looser constraints of best-fit values for N and ΔH compared to the other thiolates (see Figure S₅). However, we can make a robust comparison of the total enthalpy change per QD (ΔH per QD = $N \times \Delta H$), which is significantly more negative for MPA than for MUA. The implication is that the number

of sites, the negative enthalpy change, or both must be greater for MPA than for MUA despite the smaller equilibrium constant, which we discuss further below.

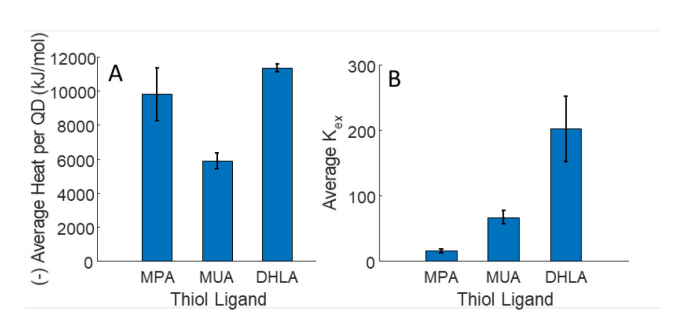


Figure 6. Average heat produced per mole QD (A) and average $K_{\rm ex}$ (B) for each QD ITC titration. Each titration was repeated in triplicate and error bars indicate 1 standard deviation

The bidentate DHLA ligand exhibited the largest $K_{\rm ex}$, and the most negative total enthalpy change, among the three ligands examined, as presented in Figure 6. The sigmoidal shape of the isotherm, corresponding to a larger c value, enables robust assignment of effective N and ΔH values. We find N is larger than for MUA and similar to the number of native oleate ligands on these QDs, while ΔH is nearly twice that for MUA. The difference in ΔH is consistent with both thiolate groups on DHLA being able bind to the QD surface. The ratio of $K_{\rm ex}$, and accordingly the difference ΔG per site, is not as large as expected given the difference in ΔH alone: rather, the more negative ΔH is partly compensated by a more negative entropy change ΔS per molecule. This can perhaps be understood in terms of the diminished conformational freedom available to DHLA when both thiolates coordinate the QD surface. The observation of a larger effective

Table 1. Thermodynamic Parameters for Thiolate Ligand Exchanges.

Thiol	N	ΔH	$K_{ m eff}$	K_{ex}	ln K _{ex}	$N\Delta H$	ΔG	$T\Delta S$
	per QD	kJ mol⁻¹	×10 ³ M ⁻¹			MJ (mol QD) -1	kJ mol⁻¹	J mol ⁻¹ K ⁻¹
MPA	148 ± 49	-68 ± 11	1.2^{a}	15 ^b	2.72 ± 0.18	-9.8 ± 1.5	-6.7 ± 0.5	-61 ± 10
	219 ± 43	[-35.8] ^c	3.0	39	3.62 ± 0.36	-7.8 ± 1.5	-9.0 ± 0.9	-26.8 ± 0.8
MUA	166 ± 26	-35.8 ± 3.0	5.4	67	4.19 ± 0.16	-4.9 ± 0.5	-10.4 ± 0.4	-25.5 ± 0.2
DHLA	200 ± 14	-56.9 ± 4.7	16.8	203	5.29 ± 0.27	-11.3 ± 0.2	-13.1 ± 0.7	-43.8 ± 5.4

^aEffective association constant in ~12 mM AEP, borate buffer, at 298 K. ^bCalculated as $K_{\text{eff}} \times [\text{AEP}]$. ^cBest fit results with ΔH held equal to the value for MUA.

number of sites *N* for DHLA versus MUA suggests that steric considerations, rather than the actual number of potential thiol coordination sites on the QD surface, may limit the achievable ligand densities.

We next sought to understand the difference in behavior between MPA and MUA in greater detail. We suspect that the initial fits of the isotherms under-estimate the ligand number at saturation (N) and over-estimate ΔH per ligand, based on several arguments. Firstly, as seen in Table 1, the initial fit requires a far more negative ΔS for exchange of AEP with MPA compared to exchange with MUA or DHLA. As the product (AEP in borate buffer) is the same in both cases, the difference in ΔS must arise from the difference in entropy change of the thiolate ligand between its state in free solution, and on the QD surface. The initial fit would require an entropic penalty for binding of MPA to the surface much greater than the one we measure for MUA. Noting that the experiment takes place below the critical micelle concentration for undecanoic acid,73 this result seems the opposite from what one might expect for confinement of the long-chain MUA to a high density monolayer, and could not be supported in preliminary statistical simulations (Mark Uline, private communication). Secondly, the Heyes group reported superior surface coverage (fewer apparent vacant sites) on CdSe/ZnS QDs coated with MPA versus DHLA,38 which would appear to suggest that N for MPA should be similar to or larger than N for DHLA. Finally, MPA and MUA possess identical functional groups and if the change in surface coordination between AEP and thiolate dominates ΔH , we would expect similar ΔH per molecule for the two, rather than the more negative ΔH for MPA emerging from the unrestricted fit. We therefore considered the values of N and K_{ex} that best describe the MPA isotherms if ΔH per site is held constant at the value obtained for MUA (-35.8 kJ/mol), resulting in curves with slightly larger residual error (see Supporting Information Figure **S6**). This result is included in **Table 1**, and finds $N\approx 220$ sites per QD with K_{ex} still significantly smaller than for MUA. In making this comparison, we emphasize that the variation in N between MPA and MUA must arise from interactions between ligands that are not explicitly accounted for in the Langmuir isotherm, such as partial occlusion of neighboring sites by the bulkier alkane chain in MUA, which was also proposed as an explanation for the observations of Heyes in comparing DHLA and MPA.

The model of identical, independent sites retains value in characterizing the measured isotherms with a minimum number of free parameters.

From previous studies of alkanethiols to Au NPs in water and alkyl thiolates to CdSe in organic solvent, 46,53 we expected that increases in chain length would be accompanied by greater exothermicity with more negative ΔH and possible compensation with more negative ΔS . In the present case we instead find the stronger binding of MUA compared to MPA requires a less negative ΔS for binding, and/or a lower ligand density at saturation (effective N) as the chain length increases between the two monodentate ligands. The stronger binding of DHLA compared to MPA appears to be driven by a more negative enthalpy change, with greater N than for MUA, emphasizing that MUA is unable to coordinate all potential thiol coordination sites on the QD, perhaps due to favored conformations in which the alkane chain obscures neighboring sites.

CONCLUSIONS

Through the application of isothermal titration calorimetry, we compared the relative binding strength of monodentate thiolate ligands, MPA and MUA, to a representative bidentate thiolate ligand, DHLA. ITC titrations conducted in the presence of a large concentration of AEP under basic conditions in borate buffer enabled us to evaluate the influence of alkyl chain length and binding group denticity in a competitive exchange. Despite the limited long-term stability of QD-AEP and QD-MPA, repeatable ITC isotherms could be obtained. Comparing the monodentate ligands, we found that greater chain length led to larger K_{ex} . This is consistent with observations of greater stability of QDs coated with longer-chain monothiolates on purification and storage in aqueous buffer.34 In thiol/oleate exchange on CdSe QDs in anhydrous solvent,⁵³ compensation between increasingly negative ΔH and ΔS led to a modest decrease in $K_{\rm ex}$ with increasing chain length. In the case of thiol adsorption to Au NPs in neutral buffer,46 similar compensation was observed. In both of these reported systems, increasing chain length led to a diminished observed number of sites, as is also seen here. While uncertainty in N precluded assigning variation in $K_{\rm ex}$ to ΔH or ΔS in the present case, the observation of increased K_{ex} with linker length is clear. Increasing the denticity of the binding group, as represented by DHLA, resulted in a much greater increase in K_{ex} ,

again consistent with generally better stability. The more negative ΔH for DHLA suggests it is indeed additional surface coordination, rather than the entropic influence of a branched chain,⁵⁷ that drives the larger $K_{\rm ex}$ for DHLA. These results have been obtained by using AEP as a common starting point for ligand exchange in homogeneous aqueous solution under mildly basic buffer conditions. The use of a weakly binding initial ligand, present in excess, succeeded in generating isotherms that could be fit and interpreted using an effective Langmuir isotherm model for ligand exchange. By utilizing zincblende colloidal CdSe/ZnS core/shell QDs, prepared with oleate ligands, the results offer a window into the relative stability of thiol-capped QDs employed for fluorescence imaging and sensing in biological contexts. These results also demonstrate the utility of ITC as a sensitive metric to evaluate ligand interactions on nanoparticle surfaces, as well as the need to further develop our understanding of how molecules bind to ODs. We anticipate that a large variety of nanocrystal ligand exchange reactions can be examined in a similar manner, and extended to physiological pH regimes through selection of appropriate reversible reactions among colloidally stable species.

ASSOCIATED CONTENT

Supporting Information. Materials; Figures S1-S23 including additional STEM images and optical spectroscopy, raw thermograms, NMR spectra; Tables S1-S2. This material is available free of charge via the Internet at http://pubs.acs.org.

AUTHOR INFORMATION

Corresponding Author

*Corresponding author. Email: greytak@sc.edu.

Present Addresses

†Present address: UES, Inc., Beavercreek, Ohio 45432, United States, and Materials and Manufacturing Directorate, Air Force Research Laboratory, Wright-Patterson AFB, Ohio 45433, United States.

Funding Sources

NSF CHE-MSN 1613388, NSF CHE-MSN 2109064, NSF IGERT 1250052.

ACKNOWLEDGMENT

This work was supported by US NSF grants CHE-MSN 1613388 and CHE-MSN 2109064. J.H.D. was additionally supported by an NSF IGERT Graduate Fellowship under grant number 1250052. We acknowledge support from the University of South Carolina through an Aspire-III grant. We thank Dr. Douglas A. Blom for assistance with electron microscopy, using the USC STEM facility supported in part by US ARO Contract W911 NF-20-1-0318. We also thank Dr. Gregory Morrison for assistance with X-ray diffraction, and Prof. Mark J. Uline for helpful discussions.

REFERENCES

(1) Dennis, A. M.; Delehanty, J. B.; Medintz, I. L. Emerging Physicochemical Phenomena along with New Opportunities at

- the Biomolecular-Nanoparticle Interface. *J. Phys. Chem. Lett.* **2016**, *7* (11), 2139–2150.
- (2) Algar, W. R.; Massey, M.; Rees, K.; Higgins, R.; Krause, K. D.; Darwish, G. H.; Peveler, W. J.; Xiao, Z.; Tsai, H.-Y.; Gupta, R.; et al. Photoluminescent Nanoparticles for Chemical and Biological Analysis and Imaging. *Chem. Rev.* **2021**, *121* (15), 9243–9358.
- (3) Medintz, I. L.; Uyeda, H. T.; Goldman, E. R.; Mattoussi, H. Quantum Dot Bioconjugates for Imaging, Labelling and Sensing. *Nat Mater* **2005**, *4* (6), 435–446.
- (4) Hildebrandt, N.; Spillmann, C. M.; Algar, W. R.; Pons, T.; Stewart, M. H.; Oh, E.; Susumu, K.; Díaz, S. A.; Delehanty, J. B.; Medintz, I. L. Energy Transfer with Semiconductor Quantum Dot Bioconjugates: A Versatile Platform for Biosensing, Energy Harvesting, and Other Developing Applications. *Chem. Rev.* **2017**, *117* (2), 536–711.
- (5) Han, H.-S.; Niemeyer, E.; Huang, Y.; Kamoun, W. S.; Martin, J. D.; Bhaumik, J.; Chen, Y.; Roberge, S.; Cui, J.; Martin, M. R.; et al. Quantum Dot/Antibody Conjugates for in Vivo Cytometric Imaging in Mice. *PNAS* **2015**, *112* (5), 1350–1355.
- (6) Talapin, D. V.; Rogach, A. L.; Kornowski, A.; Haase, M.; Weller, H. Highly Luminescent Monodisperse CdSe and CdSe/ZnS Nanocrystals Synthesized in a Hexadecylamine–Trioctylphosphine Oxide–Trioctylphospine Mixture. *Nano Lett.* 2001, *1* (4), 207–211.
- (7) Talapin, D. V.; Koeppe, R.; Götzinger, S.; Kornowski, A.; Lupton, J. M.; Rogach, A. L.; Benson, O.; Feldmann, J.; Weller, H. Highly Emissive Colloidal CdSe/CdS Heterostructures of Mixed Dimensionality. *Nano Lett.* **2003**, *3* (12), 1677–1681.
- (8) Hanifi, D. A.; Bronstein, N. D.; Koscher, B. A.; Nett, Z.; Swabeck, J. K.; Takano, K.; Schwartzberg, A. M.; Maserati, L.; Vandewal, K.; Burgt, Y. van de; et al. Redefining Near-Unity Luminescence in Quantum Dots with Photothermal Threshold Quantum Yield. *Science* 2019, 363 (6432), 1199–1202.
- (9) Ji, B.; Koley, S.; Slobodkin, I.; Remennik, S.; Banin, U. ZnSe/ZnS Core/Shell Quantum Dots with Superior Optical Properties through Thermodynamic Shell Growth. *Nano Lett.* **2020**, 20 (4), 2387–2395.
- (10) Jang, Y.; Shapiro, A.; Isarov, M.; Rubin-Brusilovski, A.; Safran, A.; Budniak, A. K.; Horani, F.; Dehnel, J.; Sashchiuk, A.; Lifshitz, E. Interface Control of Electronic and Optical Properties in IV–VI and II–VI Core/Shell Colloidal Quantum Dots: A Review. *Chem. Commun.* **2017**, 53 (6), 1002–1024.
- (11) Yakavets, I.; Francois, A.; Guiot, M.; Lequeux, N.; Fragola, A.; Pons, T.; Bezdetnaya, L.; Marchal, F. NIR Imaging of the Integrin-Rich Head and Neck Squamous Cell Carcinoma Using Ternary Copper Indium Selenide/Zinc Sulfide-Based Quantum Dots. *Cancers* 2020, 12 (12), 3727.
- (12) Jeong, S.; Achermann, M.; Nanda, J.; Ivanov, S.; Klimov, V. I.; Hollingsworth, J. A. Effect of the Thiol–Thiolate Equilibrium on the Photophysical Properties of Aqueous CdSe/ZnS Nanocrystal Quantum Dots. *J. Am. Chem. Soc.* **2005**, *127* (29), 10126–10127.
- (13) Munro, A. M.; Jen-La Plante, I.; Ng, M. S.; Ginger, D. S. Quantitative Study of the Effects of Surface Ligand Concentration on CdSe Nanocrystal Photoluminescence. *J. Phys. Chem. C* **2007**, *111* (17), 6220–6227.
- (14) Chen, Y.; Vela, J.; Htoon, H.; Casson, J. L.; Werder, D. J.; Bussian, D. A.; Klimov, V. I.; Hollingsworth, J. A. Giant Multishell CdSe Nanocrystal Quantum Dots with Suppressed Blinking. *J. Am. Chem. Soc.* **2008**, *130* (15), 5026–5027.
- (15) Greytak, A. B.; Allen, P. M.; Liu, W.; Zhao, J.; Young, E. R.; Popović, Z.; Walker, B. J.; Nocera, D. G.; Bawendi, M. G. Alternating Layer Addition Approach to CdSe/CdS Core/Shell Quantum Dots with near-Unity Quantum Yield and High on-Time Fractions. *Chem. Sci.* 2012, 3 (6), 2028–2034.

- (16) Palui, G.; Aldeek, F.; Wang, W.; Mattoussi, H. Strategies for Interfacing Inorganic Nanocrystals with Biological Systems Based on Polymer-Coating. *Chem. Soc. Rev.* **2014**, *44* (1), 193–227.
- (17) Liu, W.; Choi, H. S.; Zimmer, J. P.; Tanaka, E.; Frangioni, J. V.; Bawendi, M. Compact Cysteine-Coated CdSe(ZnCdS) Quantum Dots for in Vivo Applications. *J. Am. Chem. Soc.* **2007**, 129 (47), 14530–14531.
- (18) Susumu, K.; Uyeda, H. T.; Medintz, I. L.; Pons, T.; Delehanty, J. B.; Mattoussi, H. Enhancing the Stability and Biological Functionalities of Quantum Dots via Compact Multifunctional Ligands. *J. Am. Chem. Soc.* **2007**, *129* (45), 13987–13996.
- (19) Liu, W.; Howarth, M.; Greytak, A. B.; Zheng, Y.; Nocera, D. G.; Ting, A. Y.; Bawendi, M. G. Compact Biocompatible Quantum Dots Functionalized for Cellular Imaging. *J. Am. Chem. Soc.* **2008**, *1*30 (4), 1274–1284.
- (20) Jayaweera, N. P.; Dunlap, J. H.; Ahmed, F.; Larison, T.; Buzoglu Kurnaz, L.; Stefik, M.; Pellechia, P. J.; Fountain, A. W.; Greytak, A. B. Coordination of Quantum Dots in a Polar Solvent by Small-Molecule Imidazole Ligands. *Inorg. Chem.* 2022, *61* (28), 10942–10949.
- (21) Uyeda, H. T.; Medintz, I. L.; Jaiswal, J. K.; Simon, S. M.; Mattoussi, H. Synthesis of Compact Multidentate Ligands to Prepare Stable Hydrophilic Quantum Dot Fluorophores. *J. Am. Chem. Soc.* **2005**, *127* (11), 3870–3878.
- (22) Liu, W.; Greytak, A. B.; Lee, J.; Wong, C. R.; Park, J.; Marshall, L. F.; Jiang, W.; Curtin, P. N.; Ting, A. Y.; Nocera, D. G.; et al. Compact Biocompatible Quantum Dots via RAFT-Mediated Synthesis of Imidazole-Based Random Copolymer Ligand. *Journal of the American Chemical Society* 2010, *132* (2), 472–483.
- (23) Wang, W.; Ji, X.; Kapur, A.; Zhang, C.; Mattoussi, H. A Multifunctional Polymer Combining the Imidazole and Zwitterion Motifs as a Biocompatible Compact Coating for Quantum Dots. *J. Am. Chem. Soc.* **2015**, *137* (44), 14158–14172.
- (24) Tasso, M.; Giovanelli, E.; Zala, D.; Bouccara, S.; Fragola, A.; Hanafi, M.; Lenkei, Z.; Pons, T.; Lequeux, N. Sulfobetaine-Vinylimidazole Block Copolymers: A Robust Quantum Dot Surface Chemistry Expanding Bioimaging's Horizons. *ACS Nano* **2015**, *9* (11), 11479–11489.
- (25) Du, L.; Nosratabad, N. A.; Jin, Z.; Zhang, C.; Wang, S.; Chen, B.; Mattoussi, H. Luminescent Quantum Dots Stabilized by N-Heterocyclic Carbene Polymer Ligands. *J. Am. Chem. Soc.* **2021**, *14*3 (4), 1873–1884.
- (26) Algar, W. R.; Krull, U. J. Luminescence and Stability of Aqueous Thioalkyl Acid Capped CdSe/ZnS Quantum Dots Correlated to Ligand Ionization. *ChemPhysChem* **2007**, 8 (4), 561–568.
- (27) Breus, V. V.; Heyes, C. D.; Tron, K.; Nienhaus, G. U. Zwitterionic Biocompatible Quantum Dots for Wide PH Stability and Weak Nonspecific Binding to Cells. *ACS Nano* **2009**.
- (28) Susumu, K.; Oh, E.; Delehanty, J. B.; Blanco-Canosa, J. B.; Johnson, B. J.; Jain, V.; Hervey, W. J.; Algar, W. R.; Boeneman, K.; Dawson, P. E.; et al. Multifunctional Compact Zwitterionic Ligands for Preparing Robust Biocompatible Semiconductor Quantum Dots and Gold Nanoparticles. *Journal of the American Chemical Society* 2011, 133 (24), 9480–9496.
- (29) Chen, Y.; Cordero, J. M.; Wang, H.; Franke, D.; Achorn, O. B.; Freyria, F. S.; Coropceanu, I.; Wei, H.; Chen, O.; Mooney, D. J.; et al. A Ligand System for the Flexible Functionalization of Quantum Dots via Click Chemistry. *Angewandte Chemie International Edition* **2018**, 57 (17), 4652–4656.
- (30) Yildiz, I.; McCaughan, B.; Cruickshank, S. F.; Callan, J. F.; Raymo, F. M. Biocompatible CdSe–ZnS Core–Shell Quantum Dots Coated with Hydrophilic Polythiols. *Langmuir* **2009**, 25 (12), 7090–7096.

- (31) Shen, Y.; Roberge, A.; Tan, R.; Gee, M. Y.; Gary, D. C.; Huang, Y.; Blom, D. A.; Benicewicz, B. C.; Cossairt, B. M.; Greytak, A. B. Gel Permeation Chromatography as a Multifunctional Processor for Nanocrystal Purification and On-Column Ligand Exchange Chemistry. *Chemical Science* **2016**, *7* (9), 5671–5679.
- (32) Aldana, J.; Wang, Y. A.; Peng, X. Photochemical Instability of CdSe Nanocrystals Coated by Hydrophilic Thiols. *J. Am. Chem. Soc.* **2001**, *123* (36), 8844–8850.
- (33) Munro, A. M.; Ginger, D. S. Photoluminescence Quenching of Single CdSe Nanocrystals by Ligand Adsorption. *Nano Lett.* **2008**, *8* (8), 2585–2590.
- (34) Heyne, B.; Arlt, K.; Geßner, A.; Richter, A. F.; Döblinger, M.; Feldmann, J.; Taubert, A.; Wedel, A. Mixed Mercaptocarboxylic Acid Shells Provide Stable Dispersions of InPZnS/ZnSe/ZnS Multishell Quantum Dots in Aqueous Media. *Nanomaterials* 2020, *10* (9), 1858.
- (35) Soo Choi, H.; Liu, W.; Misra, P.; Tanaka, E.; Zimmer, J. P.; Itty Ipe, B.; Bawendi, M. G.; Frangioni, J. V. Renal Clearance of Quantum Dots. *Nat Biotech* **2007**, *25* (10), 1165–1170.
- (36) Soheyli, E.; Sahraei, R.; Nabiyouni, G.; Nazari, F.; Tabaraki, R.; Ghaemi, B. Luminescent, Low-Toxic and Stable Gradient-Alloyed Fe:ZnSe(S)@ZnSe(S) Core:Shell Quantum Dots as a Sensitive Fluorescent Sensor for Lead Ions. *Nanotechnology* **2018**, 29 (44), 445602.
- (37) Zhu, Z.-J.; Yeh, Y.-C.; Tang, R.; Yan, B.; Tamayo, J.; Vachet, R. W.; Rotello, V. M. Stability of Quantum Dots in Live Cells. *Nat Chem* **2011**, 3 (12), 963–968.
- (38) Takeuchi, H.; Omogo, B.; Heyes, C. D. Are Bidentate Ligands Really Better than Monodentate Ligands For Nanoparticles? *Nano Lett.* 2013, 13 (10), 4746–4752.
- (39) Westmoreland, D. E.; Nap, R. J.; Arcudi, F.; Szleifer, I.; Weiss, E. A. PH-Dependent Structure of Water-Exposed Surfaces of CdSe Quantum Dots. *Chem. Commun.* **2019**, *55* (38), *5435-5438*.
- (40) Arcudi, F.; Westmoreland, D. E.; Weiss, E. A. Colloidally Stable CdS Quantum Dots in Water with Electrostatically Stabilized Weak-Binding, Sulfur-Free Ligands. *Chemistry A European Journal* **2019**, 25 (63), 14469–14474.
- (41) Draczkowski, P.; Matosiuk, D.; Jozwiak, K. Isothermal Titration Calorimetry in Membrane Protein Research. *Journal of Pharmaceutical and Biomedical Analysis* **2014**, *87* (Supplement C), 313–325.
- (42) Dlouhy, A. C.; Li, H.; Albetel, A.-N.; Zhang, B.; Mapolelo, D. T.; Randeniya, S.; Holland, A. A.; Johnson, M. K.; Outten, C. E. The Escherichia Coli BolA Protein IbaG Forms a Histidine-Ligated [2Fe-2S]-Bridged Complex with Grx4. *Biochemistry* 2016, 55 (49), 6869–6879.
- (43) Falconer, R. J. Applications of Isothermal Titration Calorimetry the Research and Technical Developments from 2011 to 2015. *Journal of Molecular Recognition* 2016, 29 (10), 504–515.
- (44) Winiewska, M.; Bugajska, E.; Poznański, J. ITC-Derived Binding Affinity May Be Biased Due to Titrant (Nano)-Aggregation. Binding of Halogenated Benzotriazoles to the Catalytic Domain of Human Protein Kinase CK2. *PLOS ONE* **2017**, *12* (3), e0173260.
- (45) Prozeller, D.; Morsbach, S.; Landfester, K. Isothermal Titration Calorimetry as a Complementary Method for Investigating Nanoparticle-Protein Interactions. *Nanoscale* **2019**, *11* (41), 19265–19273.
- (46) Ravi, V.; Binz, J. M.; Rioux, R. M. Thermodynamic Profiles at the Solvated Inorganic-Organic Interface: The Case of Gold-Thiolate Monolayers. *Nano Lett.* **2013**, *13* (9), 4442–4448.
- (47) Abiodun, S. L.; Gee, M. Y.; Greytak, A. B. Combined NMR and Isothermal Titration Calorimetry Investigation Resolves Conditions for Ligand Exchange and Phase Transfor-

- mation in CsPbBr₃ Nanocrystals. *J. Phys. Chem. C* **2021**, *125* (32), 17897–17905.
- (48) Calvin, J. J.; Swabeck, J. K.; Sedlak, A. B.; Kim, Y.; Jang, E.; Alivisatos, A. P. Thermodynamic Investigation of Increased Luminescence in Indium Phosphide Quantum Dots by Treatment with Metal Halide Salts. *J. Am. Chem. Soc.* **2020**, *142* (44), 18897–18906.
- (49) Calvin, J. J.; O'Brien, E. A.; Sedlak, A. B.; Balan, A. D.; Alivisatos, A. P. Thermodynamics of Composition Dependent Ligand Exchange on the Surfaces of Colloidal Indium Phosphide Quantum Dots. *ACS Nano* 2021, 15 (1), 1407–1420.
- (50) Calvin, J. J.; Ben-Moshe, A.; Curling, E. B.; Brewer, A. S.; Sedlak, A. B.; Kaufman, T. M.; Alivisatos, A. P. Thermodynamics of the Adsorption of Cadmium Oleate to Cadmium Sulfide Quantum Dots and Implications of a Dynamic Ligand Shell. *J. Phys. Chem. C* 2022.
- (51) Jharimune, S.; Sathe, A. A.; Rioux, R. M. Thermochemical Measurements of Cation Exchange in CdSe Nanocrystals Using Isothermal Titration Calorimetry. *Nano Lett.* **2018**, *18* (11), 6795–6803.
- (52) Gee, M. Y.; Shen, Y.; Greytak, A. B. Isothermal Titration Calorimetry Resolves Sequential Ligand Exchange and Association Reactions in Treatment of Oleate-Capped CdSe Quantum Dots with Alkylphosphonic Acid. *J. Phys. Chem. C* 2020, *124* (43), 23964–23975.
- (53) Elimelech, O.; Aviv, O.; Oded, M.; Banin, U. A Tale of Tails: Thermodynamics of CdSe Nanocrystal Surface Ligand Exchange. *Nano Lett.* **2020**, 20 (9), 6396–6403.
- (54) Williams, E. S.; Major, K. J.; Tobias, A.; Woodall, D.; Morales, V.; Lippincott, C.; Moyer, P. J.; Jones, M. Characterizing the Influence of TOPO on Exciton Recombination Dynamics in Colloidal CdSe Quantum Dots. *J. Phys. Chem. C* **2013**, *117* (8), 4227–4237.
- (55) Shen, Y.; Tan, R.; Gee, M. Y.; Greytak, A. B. Quantum Yield Regeneration: Influence of Neutral Ligand Binding on Photophysical Properties in Colloidal Core/Shell Quantum Dots. *ACS Nano* **2015**, *9* (3), 3345–3359.
- (56) Freyer, M. W.; Lewis, E. A. Isothermal Titration Calorimetry: Experimental Design, Data Analysis, and Probing Macromolecule/Ligand Binding and Kinetic Interactions. In *Methods in Cell Biology*; Biophysical Tools for Biologists, Volume One: In Vitro Techniques; Academic Press, 2008; Vol. 84, pp 79–113.
- (57) Elimelech, O.; Aviv, O.; Oded, M.; Peng, X.; Harries, D.; Banin, U. Entropy of Branching Out: Linear versus Branched Alkylthiols Ligands on CdSe Nanocrystals. *ACS Nano* **2022**, *16* (3), 4308–4321.
- (58) Owen, J. S.; Park, J.; Trudeau, P.-E.; Alivisatos, A. P. Reaction Chemistry and Ligand Exchange at Cadmium–Selenide Nanocrystal Surfaces. *J. Am. Chem. Soc.* **2008**, *130* (37), 12279–12281.
- (59) Thompson, C. M.; Kodaimati, M.; Westmoreland, D.; Calzada, R.; Weiss, E. A. Electrostatic Control of Excitonic Energies and Dynamics in a CdS Quantum Dot through Reversible Protonation of Its Ligands. *J. Phys. Chem. Lett.* **2016**, *7* (19), 3954–3960.
- (60) Calzada, R.; Thompson, C. M.; Westmoreland, D. E.; Edme, K.; Weiss, E. A. Organic-to-Aqueous Phase Transfer of Cadmium Chalcogenide Quantum Dots Using a Sulfur-Free Ligand for Enhanced Photoluminescence and Oxidative Stability. *Chem. Mater.* 2016, 28 (18), 6716–6723.
- (61) Grossoehme, N.; Spuches, A.; Wilcox, D. Application of Isothermal Titration Calorimetry in Bioinorganic Chemistry. *Journal of Biological Inorganic Chemistry* **2010**, *15* (8), 1183–1191.
- (62) Morris-Cohen, A. J.; Malicki, M.; Peterson, M. D.; Slavin, J. W. J.; Weiss, E. A. Chemical, Structural, and Quantitative Analysis of the Ligand Shells of Colloidal Quantum Dots. *Chem. Mater.* **2013**, 25 (8), 1155–1165.

- (63) Liu, D.; Snee, P. T. Water-Soluble Semiconductor Nanocrystals Cap Exchanged with Metalated Ligands. *ACS Nano* **2011**, 5 (1), 546–550.
- (64) Singh, S.; Leemans, J.; Zaccaria, F.; Infante, I.; Hens, Z. Ligand Adsorption Energy and the Postpurification Surface Chemistry of Colloidal Metal Chalcogenide Nanocrystals. *Chem. Mater.* **2021**, 33 (8), 2796–2803.
- (65) Tan, R.; Shen, Y.; Roberts, S. K.; Gee, M. Y.; Blom, D. A.; Greytak, A. B. Reducing Competition by Coordinating Solvent Promotes Morphological Control in Alternating Layer Growth of CdSe/CdS Core/Shell Quantum Dots. *Chem. Mater.* **2015**, *27* (21), 7468–7480.
- (66) Greytak, A. B.; Tan, R.; Roberts, S. K. Prospects for Rational Control of Nanocrystal Shape Through Successive Ionic Layer Adsorption and Reaction (SILAR) and Related Approaches. In *Anisotropic and Shape-Selective Nanomaterials: Structure-Property Relationships*; Hunyadi Murph, S. E., Larsen, G. K., Coopersmith, K. J., Eds.; Nanostructure Science and Technology; Springer International Publishing: Cham, 2017; pp 169–232.
- (67) Kuno, M. K. Band Edge Spectroscopy of CdSe Quantum Dots. Thesis, Massachusetts Institute of Technology, 1998.
- (68) Tan, R.; Blom, D. A.; Ma, S.; Greytak, A. B. Probing Surface Saturation Conditions in Alternating Layer Growth of CdSe/CdS Core/Shell Quantum Dots. *Chem. Mater.* **2013**, 25 (18), 3724–3736.
- (69) Beaumont, P. C.; Johnson, D. G.; Parsons, B. J. Photophysical Properties of Laser Dyes: Picosecond Laser Flash Photolysis Studies of Rhodamine 6G, Rhodamine B and Rhodamine 101. J. Chem. Soc., Faraday Trans. 1993, 89 (23), 4185–4191.
- (70) Gao, Y.; Peng, X. Crystal Structure Control of CdSe Nanocrystals in Growth and Nucleation: Dominating Effects of Surface versus Interior Structure. *J. Am. Chem. Soc.* **2014**, *136* (18), 6724–6732.
- (71) Roberge, A.; Dunlap, J. H.; Ahmed, F.; Greytak, A. B. Size-Dependent PbS Quantum Dot Surface Chemistry Investigated via Gel Permeation Chromatography. *Chem. Mater.* 2020, 32 (15), 6588–6594.
- (72) Hens, Z.; Martins, J. C. A Solution NMR Toolbox for Characterizing the Surface Chemistry of Colloidal Nanocrystals. *Chem. Mater.* **2013**, 25 (8), 1211–1221.
- (73) Mukerjee, P.; Mysels, K. J. *Critical Micelle Concentrations of Aqueous Surfactant Systems*; US Government Printing Office: Washington, DC, 1971.

TOC Graphic:

